20th International Conference on Structural Mechanics in Reactor Technology (SMiRT 20)
Espoo, Finland, August 9-14, 2009
SMiRT 20-Division I, Paper 1703

Local Failure Criteria for Wall-Thinning Defect in Piping Components based on Simulated Specimen and Real-Scale Pipe Tests

Jin Weon Kim[a], Chi Yong Park[b], and Sung Ho Lee[b]

[a]Department of Nuclear Engineering, University, Gwangju, Republic of Korea, e-mail: jwkim@chosun.ac.kr
[b]Nuclear Power Laboratory, Korea Electric Power Research Institute, Daejon, Republic of Korea

Keywords: Local Failure Criteria, Wall-Thinning Defect, Notched Bar Specimen, Failure Pressure, Integrity Assessment

ABSTRACT

This study performed a series of tensile tests using notched bar specimen with various notch radii and conducted associated finite element (FE) simulations to evaluate the stress and strain states in the notched section at the points of maximum load and final failure of each specimen. From the results, local failure criteria to be able to predict maximum load carrying capacity and final failure of ductile material were derived as form of equivalent stress and strain which are considered stress triaxiality, respectively. The reliability of the criteria was verified by applying them to the evaluation of maximum load and final failure of grooved plate specimen tensile tests. Also their applicability was confirmed using the results of real-scale pipe burst test. It showed that the proposed stress and strain based criteria accurately estimate the maximum load and final failure of grooved-plate specimens, respectively. The stress based criterion, given by true ultimate tensile stress, well predicted the failure pressure of local wall-thinned pipe, while the stress modified strain based criterion overestimated the failure pressure. Therefore, it is confirmed that the simple stress based criterion is appropriate as a local failure criterion for assessing the integrity of local wall-thinned piping components subjected to internal pressure.

1 INTRODUCTION

Local wall-thinning due to flow accelerated corrosion (FAC) is now considered to be a main degradation mechnism of carbon steel piping components in nuclear power plants (NPPs) (Deardorff and Bush, 1990; Chexal et al., 1998; Michel et al., 2001). Integrity evaluation of piping components with such a wall-thinning defect is getting more attention because the integrity of the piping system directly affects the safety and operability of NPP. Since 1990s, a number of experimental and numerical studies conducted to develop an integrity assessment procedure and acceptance criteria for piping components with a local wall-thinning (Deardorff and Bush, 1990; JAERI, 1993; Roy et al, 1997; Miyazaki et al., 1999; Wilkowski et al., 2000; Choi et al., 2003; Kim and Park, 2003a; Shim et al., 2003; Oh et al., 2007), and they proposed several assessment procedures for local wall-thinned piping components. It was revealed that the assessment result of local wall-thinned piping components depends on the geometries of pipe and defect, the failure criterion, and the type of loading. Especially, the failure criterion is important in the numerical analysis based integrity assessment because it directly affects the assessment result and depends on material characteristics, loading type, defect geometry, and failure mode (Roy et al, 1997; Wilkowski et al., 2000; Oh et al, 2007).

Typically, two types of failure criteria, global and local criteria, are used for the assessment of local wall-thinned piping components (Roy et al, 1997; Oh et al, 2007). The global criteria consider general collapse of pipe by global plastic instability that is based on averge stresses in the net-section, whereas the local criteria are based on the stress and strain increments in the local wall-thinned area. In this case the local stress and strain are used as failure criteria for a local wall-thinning (Fu and Kirkwood, 1995; (Roy et al, 1997; Choi et al., 2003; Kim and Park, 2003b; Shim et al., 2003; Oh et al, 2007; Chiodo and Ruggieri, 2009). The local strain criterion assumes that the failure occurs when the maximum principle strain or equivalent strain in the local wall-thinned area exceeds a critical strain that is given as a function of stress triaxiality. It

is known that this type of strain criterion is theoreically sound, but it is difficult to obtain the stress modified critical strain of material because it needs a number of specimen tests and associated finite element (FE) analyses. For the local stress criteria, it is assumed that the failure occurs when the equivalent stress over the defect ligament reaches a critical stress that is usually defined as a fraction of the yield stress (σ_y), flow stress (σ_f), ultimate tensile stress (σ_u), and true ultimate tensile stress (σ_{ut}). Due to the simplysity in terms of application, a number of studies suggested this type of failure criterion for assessing integrity of local wall-thinned piping components (Fu and Kirkwood, 1995; Choi et al., 2003; Kim and Park, 2003b; Shim et al., 2003; Chiodo and Ruggieri, 2009). However, there was no consideration about the stress triaxiality at defected area, which is an important parameter on ductile failure of material, in the detemination of these stress based criteria.

The objective of this study is to develop the local failure criteria, which have a sound theoretical basis on the ductile failure of material and an appropriate accuracy in the integrity assessment of local wall-thinned piping components. A series of tensile tests were performed using notched bar specimens with various notch radii. Then, detailed elastic-plastic FE analyses were performed to evaluate the stress and strain states in the notched section of specimen during plastic deformation. The equivalent stress and strain at the points of maximum load and final failure were obtained by combining experimental with FE results, and the stress and strain based failure criteria were derived as a function of stress triaxilaity. The reliability of these criteria was verified by employing them to the estimation of maximum load and final failure of grooved plate specimens under tensile load and to the estimation of failure pressure of local wall-thinned pipe specimens under internal pressure.

2 DEVELOPMENT OF LOCAL FAILURE CRITERIA

2.1 Notched bad specimen tests

To obtain load and displacement data involving stress triaxiality effect on deformation behavior and ductile failure of material, a series of tensile tests were performed using notched bar specimen with various notch radii including smooth and V-notch. The specimens were machined from a carbon steel pipe of 100A Sch.80 (D_{nom}=114.3 mm, t_{nom}=8.9 mm), designated by ASTM A106 Gr.B that is commonly used in secondary piping system of NPP, which is the same one used in real-scale pipe tests for verification of local failure criteria. Figure 1 depicts the tensile specimens used in the test. The minimum section of all specimens has a diameter of 3.0mm. For notched bar specimens, five different notch radii were regarded: V-notch with notch radius (R_n) of 0.5 mm and round notch with R_n = 1.5, 3.0, 12.0, 24.0 mm.

All tests were conducted under a displacement-controlled tensile loading with a displacement rate of 0.5 mm/min at ambient temperature. In the test, displacement was measured by extensometer with gauge length of 25 mm. Figure 2 presents the load versus displacement curves obtained from smooth and notched bar specimen tests. The discrepancy of load versus displacement curves between specimens with the same notch radius was negligible. It also showed that, as the notch radius increased, the maximum load decreased and the displacements to the maximum load and final failure increased. It is believed that the load and displacement data obtained from this experiment are reliable and well represent the effects of stress triaxiality on the ductile failure of material.

2.2 Finite element simulation

Elastic-plastic FE analyses were conducted to simulate tensile tests for smooth and notched bar specimens and to estimate the stress and strain states in the notched section of specimens corresponding to the maximum load and final failure in the load versus displacement curves. As shown in Fig. 3, two-dimensional axi-symmetric FE model (CAX8R in ABAQUS) was employed in the analyses, and the analyses were performed using commercial finite element program, ABAQUS (Hibbitt, Karlson, and Sorensen Inc., 2005). A non-linear geometry option was used for incorporating a large geometry change effect and it was assumed the material obeys the incremental plasticity theory. Figure 4 shows true stress-true strain curve used in the FE analyses. The curve was calculated from the engineering stress-strain curve of smooth tensile test data up to necking, and it was obtained using FE simulation technique beyond the onset of necking. The experimental load versus displacement curve was considered as target and true stress-true strain relation was searched for iteratively by FE simulation until the target was reached within a certain tolerance.

In the analyses displacement boundary condition was applied to the top of the FE model, and the corresponding tensile load was determined from the nodal forces. The gauge length elongation was monitored from the FE displacement results. The stress and strain in the notched section were also extracted from the FE analysis results. Figure 5 presents the comparisons of load versus displacement curves obtained from tensile tests and FE simulations. In all cases, the simulated and measured loads and displacements at the necking point were almost identical; the simulated load versus displacement curve almost completely matches with the experimental one beyond necking up to final failure, although there are some discrepancies in the specimens with small notch radius.

Therefore, it is indicated that FE analysis well simulates the results of notched bar specimen test, and thus detailed information on the stress and strain states in the notched section of specimens can be also obtained as a function of applied load. It is also believed that an appropriate local failure criterion can be drawn from these stress and strain states in the notched section of specimen.

2.3 Local failure criteria

To relate the stress and strain states in the notched section with failure of specimen, the stress and strain components were evaluated at the maximum load and final failure points on the load versus displacement curve for each specimen. In the evaluation, the stress triaxiality is defined by the ratio of the mean stress (σ_m) to the equivalent stress (σ_e):

$$\frac{\sigma_m}{\sigma_e} = \frac{\sigma_1 + \sigma_2 + \sigma_3}{3\sigma_e} \tag{1}$$

where σ_i (i=1,2,3) are the principal stresses. The equivalent stress and equivalent strain (ε_e) are defined as Eqs. (2) and (3):

$$\sigma_e = \frac{1}{\sqrt{2}}\left[(\sigma_1 - \sigma_2)^2 + (\sigma_2 - \sigma_3)^2 + (\sigma_3 - \sigma_1)^2\right]^{/2} \tag{2}$$

$$\varepsilon_e = \frac{\sqrt{2}}{3}\left[(\varepsilon_1 - \varepsilon_2)^2 + (\varepsilon_2 - \varepsilon_3)^2 + (\varepsilon_3 - \varepsilon_1)^2\right]^{/2} \tag{3}$$

At both maximum load and final failure points, the stress triaxialities in the notched section showed a non-uniform distribution, i.e., their maximum appeared at the center of notched section and the minimum appeared at the free surface, and the overall values increased with decreasing notch radius. The equivalent stress and strain at the maximum load were nearly a constant over the notched section except for V-notch specimen, and the variations of these values with notch radius were minor. However, the equivalent stress and strain at final failure point considerably varied with radial position within the notched section and their overall values increased with increasing notch radius. Since the stress and strain components showed non-uniform distributions within the notched section, the results were investigated based on averaged stress and strain over the notched section. Also, the stress triaxiality in the notched section depends strongly on the equivalent strain (Bao, 2005; Oh et al., 2007), so that it was averaged to maximum load and to final failure as shown in Eqs. (4) and (5);

$$\left(\frac{\bar{\sigma}_m}{\bar{\sigma}_e}\right)_{ave,m} = \frac{1}{\bar{\varepsilon}_{em}}\int_0^{\bar{\varepsilon}_{em}} \frac{\bar{\sigma}_m}{\bar{\sigma}_e} d\bar{\varepsilon}_e \tag{4}$$

$$\left(\frac{\bar{\sigma}_m}{\bar{\sigma}_e}\right)_{ave,f} = \frac{1}{\bar{\varepsilon}_{ef}}\int_0^{\bar{\varepsilon}_{ef}} \frac{\bar{\sigma}_m}{\bar{\sigma}_e} d\bar{\varepsilon}_e \tag{5}$$

where $\bar{\varepsilon}_{em}$ denotes the section average of equivalent strain to maximum load and $\bar{\varepsilon}_{ef}$ denotes the section average of equivalent strain to final failure.

Figure 6 presents the section average of equivalent stress at maximum load and the section average of equivalent strain at final failure evaluated from each specimen as a function of stress triaxiality. It shows that

the averaged equivalent stress at maximum load showed nearly independent of stress triaxiality in the notched section. The averaged equivalent strain at final failure exponentially decreased with increase in stress triaxiality. Therefore, the averaged equivalent stress corresponding to maximum load of specimen can be presented as a constant that is almost identical to true stress at necking point (true ultimate tensile stress, σ_{ut}), and the averaged equivalent strain corresponding to final failure of specimen can be presented by regression as a function of stress triaxiality. These are expressed as Eqs. (6) and (7);

$$\bar{\sigma}_{em} = \sigma_{ut} \tag{6}$$

$$\bar{\varepsilon}_{ef} = 0.7367\left(\frac{\bar{\sigma}_m}{\bar{\sigma}_e}\right)^{-0.9548} \tag{7}$$

Thus, the maximum load carry capacity and final failure of structurals containing a notch type defect subjected to displacement-controlled loading can be estimated by applying Eqs. (6) and (7), when the stress triaxiality and the equivalent stress and strain over the ligament are given by FE analyses. Usually it is regarded that the failure occurs under load-controlled loading condition when the applied load reaches the maximum load defined under displacement-controlled loading condition. Therefore, it can be proposed from this results that Eqs. (6) and (7) are local failure criteria for loca wall-thinning defect under load-controlled loading condition and displacement-controlled loading condition, respectively.

2.4 Verification using Grooved Plate Specimen Tests

To verify the reliability of the proposed local failure criteria, a series of tensile tests were conducted using grooved plate specimens with different groove radius, which were designed to simulate the stress states in the local wall-thinning defect. As shown in Fig. 7, the specimen contains a round groove at both sides of plate; the groove radii are 3, 6, and 24mm. From the tensile tests, the load versus displacement curves were obtained, and the loads and displacements to the maximum load and final failure points were evaluated for each specimen. In addition, FE simulations were performed on the grooved plate specimen tests to evaluate the stress states in the minimum section of grooved plate specimen for a given load level. Three-dimensional FE model (C3D20R in ABAQUS) was used in the simulation as shown in Fig. 7. Considering the geometrical symmetry of the specimen, one eighth of the full specimen was modeled. The analysis procedure was the same as that considered in the simulation of notched bar specimen tests. Figure 8 exhibits the simulated load versus displacement curve for each specimen along with experimental one.

The averaged equivalent stress and strain and the averaged stress triaxiality over the thickness at the center of groove were evaluated for a given load level from the results of FE analyses. The maximum load and final failure load for each specimen were estimated by applying the proposed criteria, Eqs. (6) and (7), to the evaluation results. Table 1 compares the estimated and experimental loads at maximum load and finial failure of specimen. It shows that the estimated maximum loads agreed well with experimental loads within 1.5% error regardless of groove radius. For most cases, moreover, the estimated maximum loads were lower than the experimental results; i.e., it provided a conservative estimation. For finial failure loads, also, the estimated results showed a good agreement within 4% error. Therefore, it is indicated that the proposed stress based and strain based criteria accurately predict the maximum load carrying capacity and final failure of grooved plate specimens, which simulate the stress states of local wall-thinning, tested under the displacement-controlled loading condition.

3 APPLICATION OF LOCAL FAILURE CRITERIA

Failure criteria based on the equivalent stress and strain were proposed as a function of the stress triaxiality and were verified using the results of grooved plate specimen tests. In this section, their applicability is confirmed by employing these criteria to the estimation of failure pressure of local wall-thinned pipe specimen.

3.1 Real-Scale Pipe Tests

A series of burst tests were conducted using pipe specimens containing a simulated local wall-thinning. As illustrated in Fig. 9, the specimens were made of ASTM A106 Gr.B carbon steel pipe of 100A Sch.80, which

is the same pipe material used in the notched bar and grooved plate specimens tests. To obtain the uniform diameter and thickness of the pipe specimen, the outer and inner surfaces were machined prior to introducing the local wall-thinning defect. After machining, the outer diameter (D_o) and thickness (t) was 112.0 mm and 6.2 mm, respectively. The local wall-thinning was made on the inside wall; its circumferential and axial shapes are circular, and then the specimen was end-capped by welding. In the experiment, four specimens with three different circumferential thinning angles for a given thinning length and thinning depth were used as listed in Table 2.

Internal pressure was monotonically applied to the specimen up to the occurrence of burst at wall-thinned area. Testing apparatus was composed of a pressurization system, testing bed, and the data acquisition system. The testing bed was designed so it could easily control the end-displacement of the specimen during pressurization; one end of the specimen was fixed by a hinge and the other end was free-sliding. Hydraulic pressure was employed to pressurize the specimen for the present experiment. The data acquisition system consisted of a data logger and a PC to capture the experimental data. In addition, two video cameras were installed in front of and on top of the specimen to monitor the deformation and burst at final stage. Thus, the internal pressure, end-displacement of the specimen, and strains at the thinned area were measured at a rate of 1 sample per second. Measured failure pressure for each specimen was summarized in Table 2. Figure 10 shows the set-up for burst tests and failure mode taken from the post-test wall-thinned pipe specimens.

3.2 Estimation of Failure Pressure

FE analyses were conducted to estimate the failure pressure of local wall-thinned pipe specimens tested. In the analyses three-dimensional elastic-plastic FE model (C3D20R in ABAQUS) was used as shown in Fig. 11. One fourth of the full specimen was modeled, based on the dimensions measured from each specimen in the experiment, considering geometrical symmetry of pipe specimen. Three elements were layered along the thickness and fine meshing was considered in the wall-thinned region. Internal pressure was applied to the inner surface of the pipe, together with end forces to simulate the closed cap condition. In the analysis non-linear geometry option was employed to account for the large deformation at wall-thinned area, and true stress-true strain curve shown in Fig. 4 was used in the analysis. The analysis was performed using ABAQUS code. From the FE analyses, the averaged equivalent stress and strain and the averaged stress triaxiality over the ligament at the center of wall-thinned area were evaluated as a function of internal pressure.

By applying the proposed local failure criteria, the failure pressures were estimated from the results of FE analyses. Figure 12 compared the estimated failure pressure with the experimental result. It showed that the local stress based criterion given by Eq. (6) provided an excellent estimation of failure pressure for local wall-thinned pipe specimens within maximum error of 5.7%, whereas the stress modified strain based criterion given by Eq. (7) showed an overestimation of failure pressure. This indicates that the simple stress based criterion, as represented by σ_{ut}, is better in the estimation of failure pressure for local wall-thinned piping components than the strain based criterion expressed by a function of stress triaxilaity. This is because the burst of local wall-thinned pipe specimen under internal pressure is a failure by load-controlled loading rather than displacement-controlled loading. Thus, it is demonstrated that the simple stress based criterion given by σ_{ut} is an appropriate local failure criterion for integrity assessment of local wall-thinned piping components subjected to simple internal pressure.

A number of studies suggested the stress based local failure criterion to assess the integrity of local wall-thinned piping components. It was reported that the local wall-thinned pipe subjected to combined internal pressure and bending load was failed when the section average of equivalent stress exceeds σ_{ut} of pipe material (Kim and Park, 2003b). Fu (1995) also proposed a stress based criterion to predict the failure of local wall-thinned area, which assumes the failure occurs by plastic collapse when the minimum equivalent stress at wall-thinned area reaches σ_{ut} of pipe material. In the previous studies, the failure criterion of σ_{ut} was derived without any consideration of stress states at wall-thinned area. The present results confirmed that the stress based criterion of σ_{ut} is less dependent on the stress triaxilaity at wall-thinned area and reliably applicable to the eastimation of failure pressure for local wall-thinned piping components.

4 CONCLUSION

(1) Two types of local failure criteria for a local wall-thinning were proposed based on the notched bar tensile tests and associated finite element simulations; one is a simple stress based criterion given by true ultimate tensile stress and the other is a strain based criterion that is a function of stress triaxiality.

(2) The comparison with grooved plate specimen tensile data showed that the stress and strain based criteria accurately estimate the maximum load and final failure of grooved plate specimens tested under displacement-controlled tensile loading, respectively.

(3) The stress based criterion well predicted the failure pressure of local wall-thinned pipe, whereas the strain based criterion overestimated the failure pressure. Thus, it is confirmed that the simple stress based criterion given as true ultimate tensile stress is reliable as a failure criterion for a local wall-thinning in the piping components subjected to simple internal pressure.

Acknowledgements. *This work has been supported by KESRI(R-2008-36), which is funded by MKE(Ministry of Knowledge Economy)*

REFERENCES

ABAQUS Users manual, version 6.5, Hibbitt, Karlson & Sorensen, 2005

Bao, Y., 2005, "Dependence of ductile crack formation in tensile tests on stress triaxiality, stress and strain ratios," *Eng. Frac. Mech.*, Vol. 72, pp. 505-522.

Chexal, B., Horowitz, J., Dooley, B., Millett, P., Wood, C., and Jones, R., 1998, "Flow-accelerated corrosion in power plant," *EPRI/TR-106611-R2.*

Chiodo, M.S.G. and Ruggieri, C., 2009, “Failure assessments of corroded pipelines with axial defects using stress-based criteria: Numerical studies and verification analyses,” Int. J. of Press. Ves, Vol. 86, pp.164-176.

Choi, J.B., Goo, B.K., Kim, J.C., Kim, .Y.J., and Kim, W.S., 2003, "Development of limit load solutions for corroded gas pipelines," *Int. J. Press. Ves. and Piping*, Vol.80, pp. 121-128.

Deardorff, A.F. and Bush, S.H., 1990, "Development of ASME section XI criteria for erosion-corrosion thinning of carbon steel piping," PVP-Vol-186, NDE-Vol. 7, pp. 71-75.

Fu, B. and Kirkwood, M.G., 1995, "Predicting failure pressure of internally corroded linepipe using the finite element method," OMAE-Vol.V, Pipeline Tech., ASME

Michel, F., Reck, H., and Schulz, H., 2001, “Experience with piping in German NPPs with respect to aging-related aspects,” Nucl. Eng. Design, 207, pp. 307～316.

Miyazaki, K., Kanno, S., Ishiwata, M., Hasegawa, K., Ahn, S.H., and Ando K., 1999, "Fracture behavior of carbon steel pipe with local wall thinning subjected to bending load," *Nucl. Eng. & Des.*, Vol. 191, pp. 195-204.

Japan Atomic energy Research Institute, 1993, "Technical report on the piping reliability tests at the Japan Atomic Energy Research Institute," JAERI-M, 93-074, pp. 104-115.

Kim, J.W. and Park, C.Y., 2003a "Effect of length of thinning area on the failure behavior of carbon steel pipe containing a defect of wall thinning," *Nucl. Eng. & Des.*, Vol. 220, pp. 274-284.

Kim, J.W. and Park, C.Y., “Criterion for failure of internally wall thinned pipe under a combined pressure and bending moment,” *Trans. of SMiRT-17*, Paper #G07-5, Prague, Czech Republic, Aug. 17-22, 2003b

Oh, C.K., Kim, Y.J., Baek J.H., and Kim, W.S., 2007, “Development of stress-modified fracture strain for ductile failure of API X65 steel,” Int. J. of Fract., Vol. 143, pp.119-133.

Roy, S., Grigory, S., Smith, M., Kannunen, M.F., and Anderson, M., 1997, "Numerical simulations of full-scale corroded pipe tests with combined loading," *J. Press. Ves. Tech.*, Vol.119, pp. 457-466.

Shim, D.J., Choi, J.B, Kim, Y.J., Kim, J.W., and Park, C.Y, 2003, "Assessment of local wall thinned pipeline under combined bending and pressure," *Int. J. Mod. Phy. B*, Vol. 17, pp. 1870-1876.

Wilkowski, G., Stephens, D., Krishnaswamy, P., Leis, B., and Rudland D., 2000, "Progress in development of acceptance criteria for local tinned areas in pipe and piping components," *Nucl. Eng. & Des.*, Vol. 195, pp. 149-169.

Table 1 Comparison of estimated and measured loads for grooved plate tests

Specimen	Load at maximum load			Load at final failure		
	Experimental [kN]	Estimated [kN]	Diff. [%]	Experimental [kN]	Estimated [kN]	Diff. [%]
R=3mm	55.30	55.18	0.23	48.17	47.02	2.38
	55.69	55.18	0.92	48.80	47.02	3.66
	55.48	55.18	0.54	47.77	47.02	1.58
R=6mm	52.40	53.13	1.39	45.72	46.13	-0.90
	52.65	52.26	0.74	45.71	45.60	0.23
	52.16	52.26	0.18	45.24	45.61	-0.81
R=24mm	48.76	48.21	1.11	43.45	41.75	3.91
	48.96	48.75	0.42	43.17	42.84	0.76
	48.38	47.90	0.99	42.64	42.12	1.22

Table 2 Wall-thinning geometries and failure pressure for each pipe specimen

Specimen	Wall-thinning geometry			Measured Failure pressure [MPa]
	Circ. thinning angle, θ/π	Thinning length, L/D_o	Thinning depth, $(t-t_p)/t$	
SP-1	0.5	1.0	0.708	24.81
SP-3	0.125	1.0	0.648	29.91
SP-4	0.25	1.0	0.635	30.81
SP-5	0.5	1.0	0.640	31.00

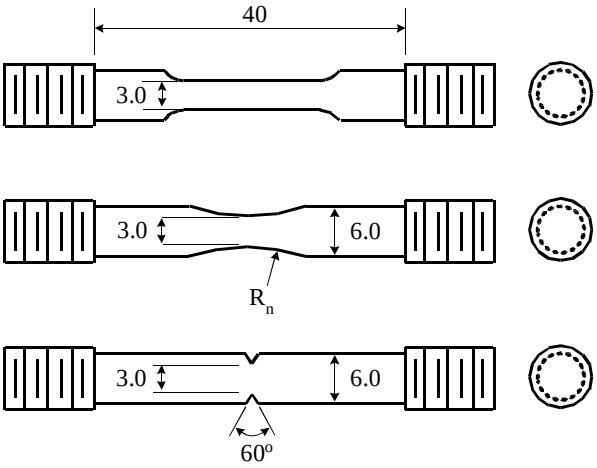

Figure 1. Geometries of notched bar specimens

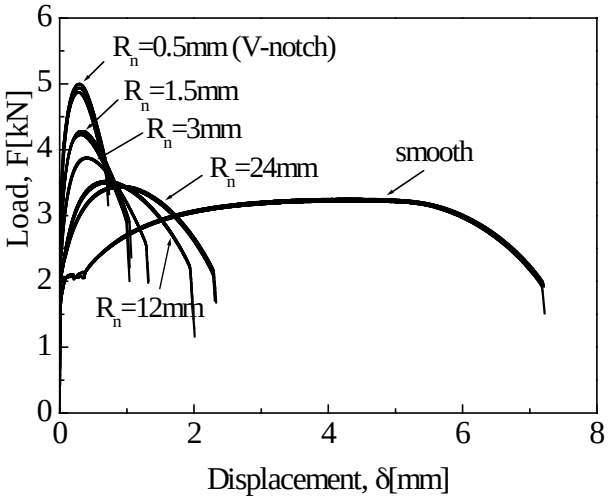

Figure 2. Load-displacement curves obtained from the tensile tests using smooth and notched bar specimens

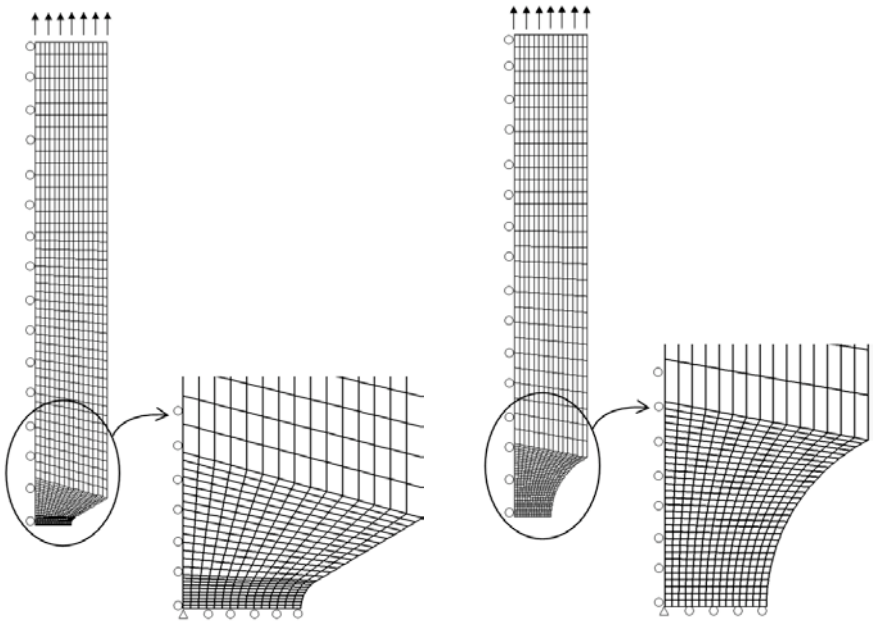

(a) V-notch (b) Round notch

Figure 3. Finite element meshes for notched bar specimens

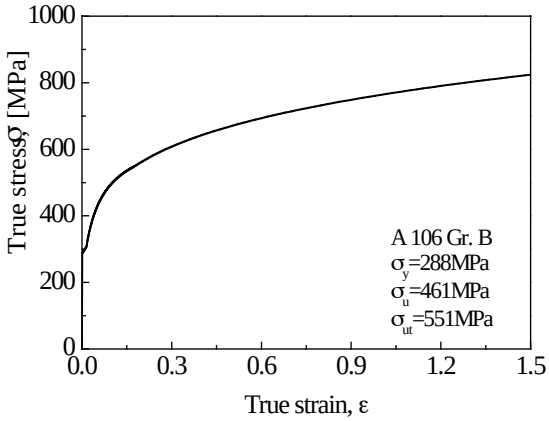

Figure 4. True stress-true strain curve used in finite element analysis

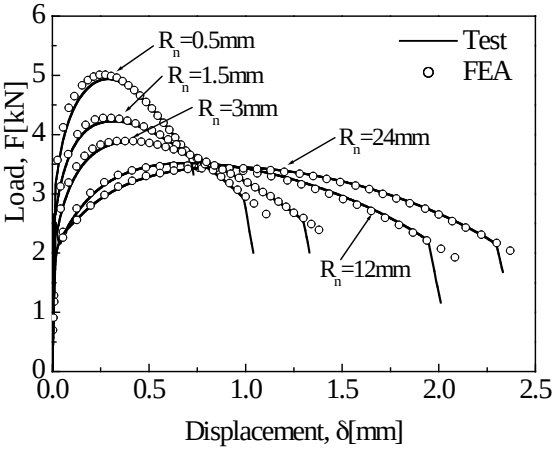

Figure 5. Comparisons of experimental with simulated load-displacement curves for notched bar specimens

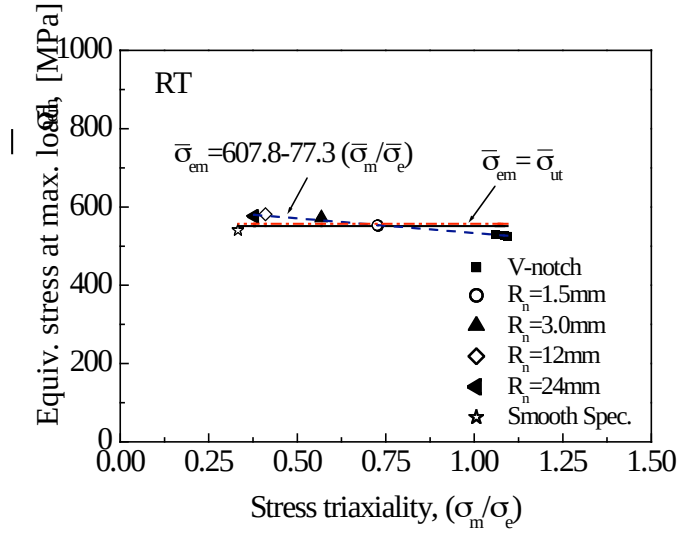

(a) At maximum load

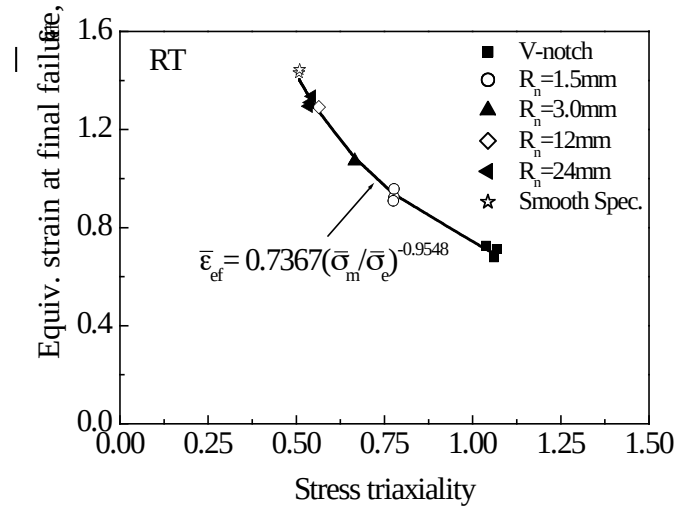

(b) At final failure

Figure 6. Averaged equivalent stress and strain corresponding to the maximum load and final failure as a function of stress triaxiality.

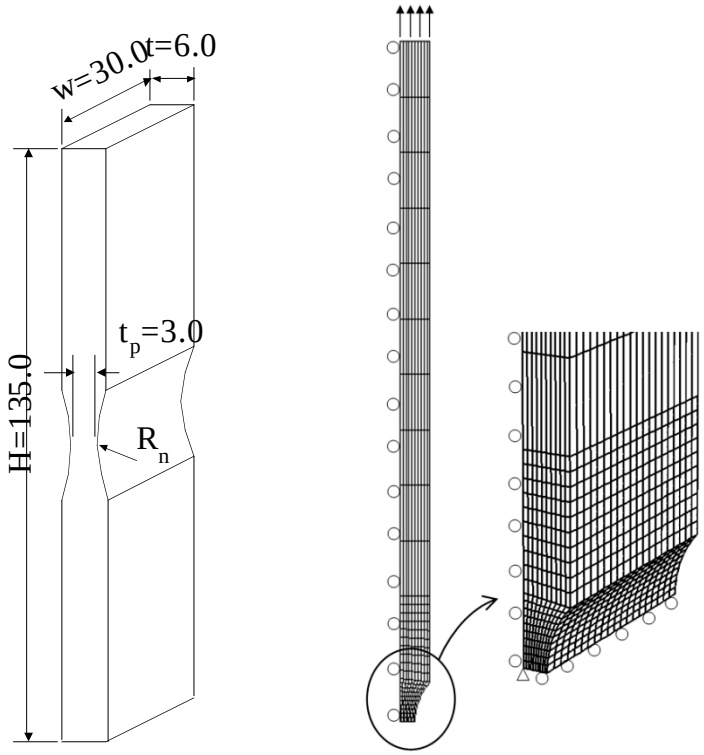

(a) Grooved plate specimen (b) FE model

Figure 7. Geometry of grooved plate specimen and its FE model

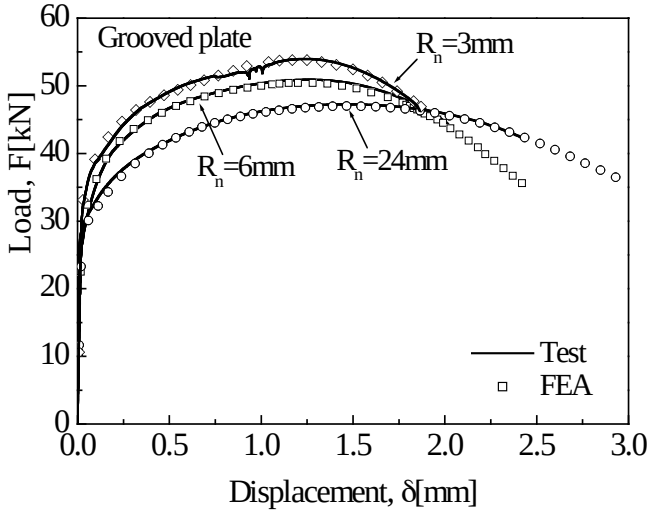

Figure 8. Comparisons of experimental with simulated load-displacement curves for grooved plate specimens

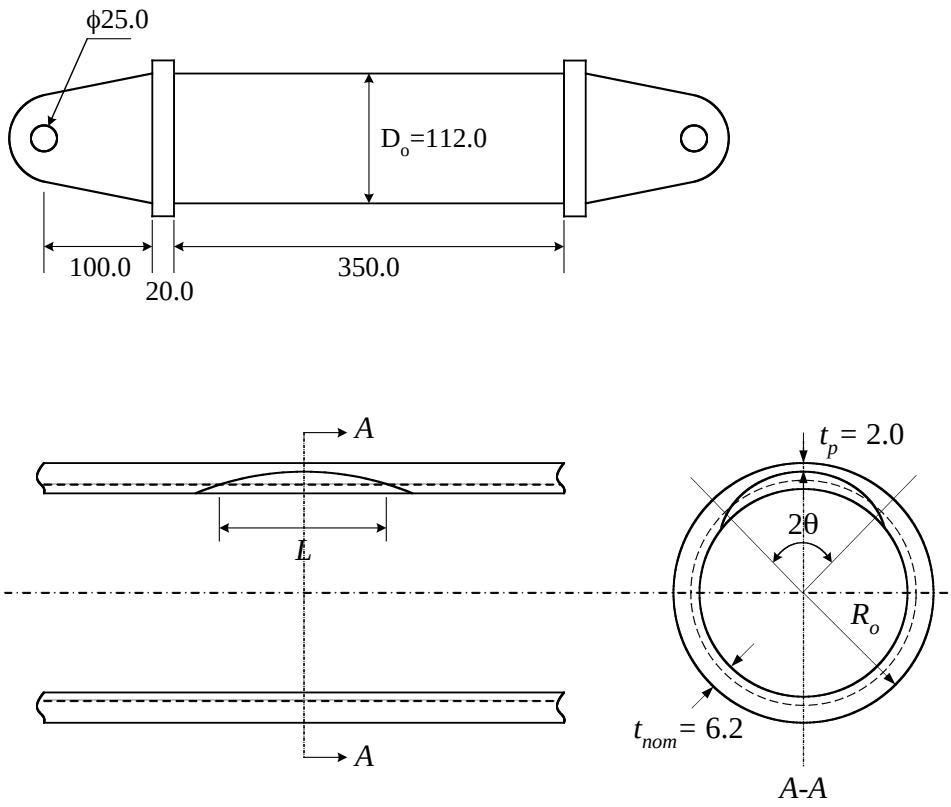

Figure 9. Geometries of local wall-thinned straight pipe

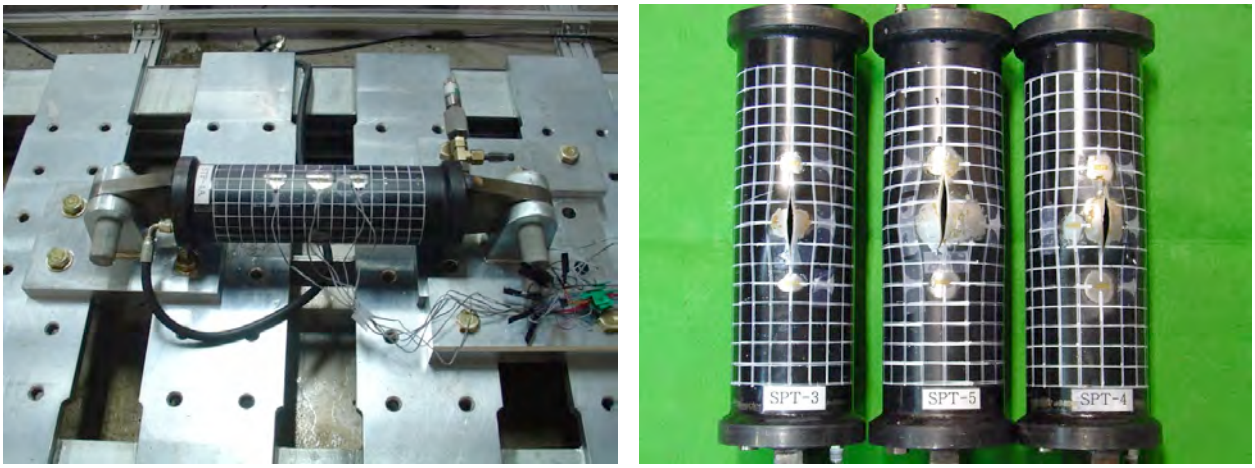

(a) Test set-up (b) Final failure mode

Figure 10. Test set-up and failure mode of local wall-thinned pipe specimens

Figure 11. FE model for local wall-thinned pipe specimen

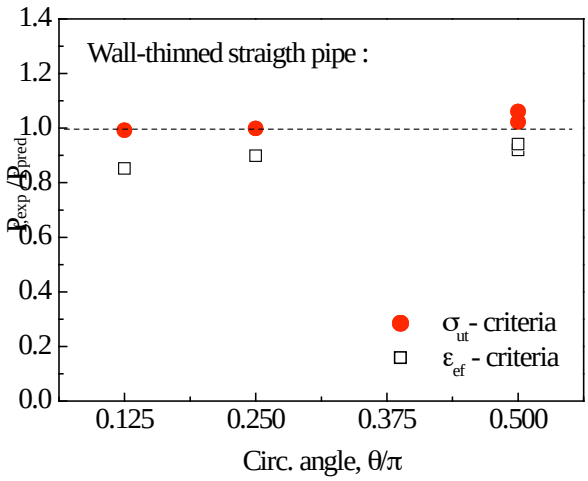

Figure 12. Comparison of experimental and estimated failure pressures of local wall-thinned straight pipe